

Black poly-silicon: a nanostructured seed layer for sensor applications

Z. Fekete¹, Á. Horváth², Zs. Bérces¹, A. Pongrácz¹

¹MEMS Lab, Institute for Technical Physics & Material Science, Research Centre for Natural Sciences, Hungarian Academy of Sciences, P.O.Box 49, H-1525 Budapest, Hungary

² Budapest University of Technology & Economics, 3 Műegyetem rkp., H-1111 Budapest, Hungary

E-mail: feketezoltan@ttk.mta.hu

Abstract:

Nanostructured silicon surfaces like black-silicon (b-Si) are of great interest in current sensor technology. This paper presents an alternative method to fabricate b-Si in poly-silicon thin film prepared on pre-deposited insulation layer in order to open new door to the integration of silicon nanograss in biosensor application as sensing or seed layer. In our experiment, black poly-silicon (BPS) is formed in LPCVD deposited poly-silicon thin film by deep reactive ion etching (DRIE) at cryogenic temperature in SF₆+O₂ plasma. Etching parameters like temperature, O₂ flow and RF power is varied and morphology of the resultant thin film is analyzed by scanning electron microscopy. The fabricated samples are subjected to a comparative investigation, which contained pillar density, directionality, etch rate and loading effects. The effect of the grain size of poly-silicon layer is analyzed and compared to samples micromachined in single-crystalline silicon (c-Si). We found that fabrication parameters of BPS morphology significantly differ from that of conventional b-Si realized in c-Si substrate. A simple application example of our BPS layer for increasing specific surface area of potential sensors is also demonstrated. As far as we know, this is the first demonstration and systematic study of b-Si fabrication in poly-silicon thin film.

Key words: Si nanograss, black-silicon, b-Si, Si nanopillar, Si nanorod, Si whiskers, black poly-silicon, nanostructures

1. Introduction

Black-silicon (b-Si) is an array of nanopillars formed in silicon substrate by microfabrication methods. First formations of b-Si dates back to the mid 90's [Jansen, 1995], however, its direct fabrication and integration into photovoltaics, optics and special MEMS applications have begun only some years ago. Due to its high absorption in the visible and infrared wavelengths several demonstrations took place in the development of solar cells as black nonreflective surfaces to minimize reflection losses [Koykov, 2006; Yoo, 2006]. Hoyer et al. [Hoyer, 2008] reports that the black Si surface structure, in contrast to expectations for indirect semiconductors, shows an emission in the terahertz range using optical excitation [Hoyer, 2008]. Besides unique optical properties, several applications have shown its versatility in the recent past as superhydrophobic structure with self-cleaning features [Barbareglou, 2010; Zhang, 2013], as superhydrophilic layer with the help of a polymer monolayer attachment [Dorrer 2008] or as mechanical interface for promoting silicon-polymer bonding

[Stubenrauch, 2006]. Utilizing the high effective surface area of silicon nanograss, impedance measurement-based biosensor was developed for label free detection of cells in cancer research [Mohammad, 2014]. Metal coated b-Si surfaces have opened the door to various other applications, too. Ag coated leaning b-Si nanopillars were used as analyte trapping substrate for surface enhanced Raman scattering (SERS) and was proposed as a candidate for further explosive sensor development [Schmidt, 2012]. Gold covered Si nanopillar forests were used as a microfluidic SERS active biosensor structure [Haiyang, 2011].

The indirect appearance of b-Si grass was first observed as an undesirable side effect during chlorine based [Oehrlein, 1990] and fluorine based [Legtenberg, 1995] reactive plasma etching of silicon. Later on, utilizing the advantageous properties of the nanostructured Si surface, controlled fabrication of b-Si in single crystalline silicon substrate was reported. With proper parameter settings the two most commonly used fluorine-based DRIE methods, the so-called Bosch-process and also the cryogenic or mixed-mode result in the formation of b-Si [Jansen, 1995; Jansen, 2009; Jansen, 2010]. Reactive ion etching (RIE) in CF_4 [Gharghi, 2006], in Cl_2 [Kalem, 2011] or SF_6 plasma [Stubenrauch, 2006; Yoo, 2006; Dorrer, 2008; Hoyer, 2008] have been used to realize Si nanograss. Wet chemistry based on the local catalytic action of nanometer-sized Au dots [Koynov, 2006, Zhang2013, Su2012] or laser direct writing [Serpenguzel, 2008; Barberoglou, 2010; Vorobyev, 2011] have also been reported as a reliable tool for Si nanograss formation.

In spite of intensive investigations on c-Si nanograss, its formation mechanism is still not properly understood. During the RIE process, it is supposed that the formation of b-Si nanograss is caused by the local variation of the Si etch rate. The more likely cause of this variation is a micromasking phenomenon, where redeposition of the masking material occurs. A speculative model in the case of c-Si etched in SF_6 plasma is reported by Jansen et al. [Jansen, 2010].

In this paper, an alternative MEMS-compatible approach to nanostructure sensor surfaces is proposed using deposited poly-Si thin film as a base layer for b-Si formation. The advantages of our method are the following:

- (i) The proposed large area maskless nanofabrication can be easily combined with the conventional photolithography and integrated into the standard silicon based process flows. Compared to the limitations of black c-Si fabrication, nanostructured surfaces can be formed on top of insulator layers allowing the design and fabrication of more complex sensor structures.
- (ii) Nanoscale morphology of a sensor surface can be tailored to the physical, chemical, optical or biological requirements by tuning the thickness and morphology of BPS seed layer and the etching parameters.

As far as we know, this is the first time that b-Si formation in poly-Si thin film was investigated. Our work summarizes the effect of relevant fabrication parameters on the morphology of BPS. The fabrication steps are integrated in the process flow of a potential sensor as an example. A basic application of BPS layer utilizing the increased specific surface area is demonstrated.

2. Experimental

2.1 Black poly-silicon fabrication

Sample fabrication is based on a silicon surface micromachining process detailed in Fig 1. 500nm thick thermal SiO₂ is grown on a (100) oriented silicon wafer. 1000nm thick poly-Si is deposited in a Tempres LPCVD equipment at 250 sccm flow of SiH₄ gas at temperatures of 630°C and 610°C. Micropatterning of poly-Si was performed by photolithography and subsequent etching in poly-etchant (HF:HNO₃:CH₃COOH = 3:2:5) for 10 minutes. Black-Silicon formation was carried out in an Oxford Plasmalab 100 deep reactive ion etching chamber in mixed mode at cryogenic temperature. In order to avoid crack generation in the patterned photoresist, a 40-minute-long post-bake at 150°C is performed right after developing the pattern. Before dry etching of the samples, a preliminary conditioning of each tested recipe for 1 minute was conducted in the cooled chamber which was initially handled by 10 minutes etching of a dummy wafer in SF₆ plasma and 45 minutes in O₂ plasma for ensure better reproducibility. Relevant etching parameters and sample types are summarized in Table 1. In the latter paragraphs, poly-Si "A" and "B" denote deposition temperature (630°C and 610°C respectively) of poly-silicon thin film.

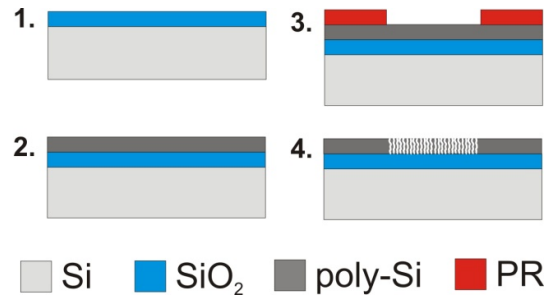


Figure 1: Process scheme for BPS fabrication (a.). Figure is not to scale.

Samples	O ₂ flow (sccm)	SF ₆ flow (sccm)	Chamber pressure (mTorr)	Time (min)	T (°C)	P _{RF} (W)	P _{ICP} (W)	loading (%)
c-Si, poly-Si "A" and "B"	10, 15	40	40	1	-110 -100 -90	2, 3	700	10, 90

Table 1: Summary of dry etching parameters

The exposed area defined by photolithography is 10% in case of all samples except for the particular one (90%) used for demonstrating the effect of macroloading.

2.2 Morphology characterization

Morphology of nanopatterned surfaces was analyzed by scanning electron microscopy (LEO 1540) and subsequent evaluation with ImageJ software was performed. In our investigations we used two quantitative parameters to reveal the relationships between micromachining parameters and morphology: pillar density and pillar height. Pitch density corresponds to the number of spot-like contaminations on the surface exposed to DRIE and normalized to $1 \mu\text{m}^2$. Eventually this pitch density is equal to BPS pillar density as etching proceeds. Pillar height refers to the average height of BPS nanopillars, which also features the etch rate of the original layer. To identify pillar density, SEM micrographs were acquired at 30° tilt angle. Cross-sectional views at 10° tilt angle were used to measure pillar height. Each parameter was derived from the evaluation of at least three micrographs.

Besides quantitative measurements, a qualitative analysis was also done focusing on the effect of crystalline compounds in the initial materials and on the loading effects. The surface of the polycrystalline layers was characterized by SmartSPM 100 atomic force microscope and RMS roughness data were derived. The ratio of crystalline compounds was evaluated by XRD analysis with a Bruker AXS D8 Discover diffractometer. The influence of exposed area in the macro- and microscale was also investigated through SEM pictures.

2.3 Specific surface area and impedance measurement

The specific surface of the nanopatterned silicon samples were evaluated by cyclic voltammetry (CV) and impedance reduction was detected by electrochemical impedance spectroscopy (EIS) measurements. 100 nm of platinum was sputtered on BPS samples of 0.25 cm^2 with an adhesion layer of 15 nm Ti in a DC sputtering equipment. Both CV and EIS measurements were performed in three electrode compartment using an Ag/AgCl reference electrode and a counter electrode of platinum wire. 0.5 M H_2SO_4 solution and lactated Ringer's solutions were used as electrolytes for CV and EIS, respectively. Reference 600 (Gamry Instruments, PA, USA) potentiostat, Gamry Framework 6.02 and Echem Analyst 6.02 were used for experimental control, data collection and analysis. Experiments were performed in a Faraday cage. Sweep rate of 500 mV/s was applied. The probe signal was sinusoidal, 25 mV RMS. The specific surface area of the recording sites was computed from the CV curves and was compared.

3 Results

3.1 Effect of etching parameters

3.1.1 Temperature

Generally, wafer temperature (or stage temperature) is responsible for rate of SiF_xO_y layer formation [Pereira, 2009]. Since a previous study proved that decreasing the wafer temperature down to -130°C causes SF_6 condensation and orientation dependant etching mechanism [Walker, 2001], we kept temperature well above -120°C . Generally, the temperature range between -90°C and -115°C is found to be optimal for the formation of more vertical micro- and nanostructures [Jiang, 2012].

Temperature sensitivity of our proposed microfabrication method is represented by Fig. 2 and Table 2.

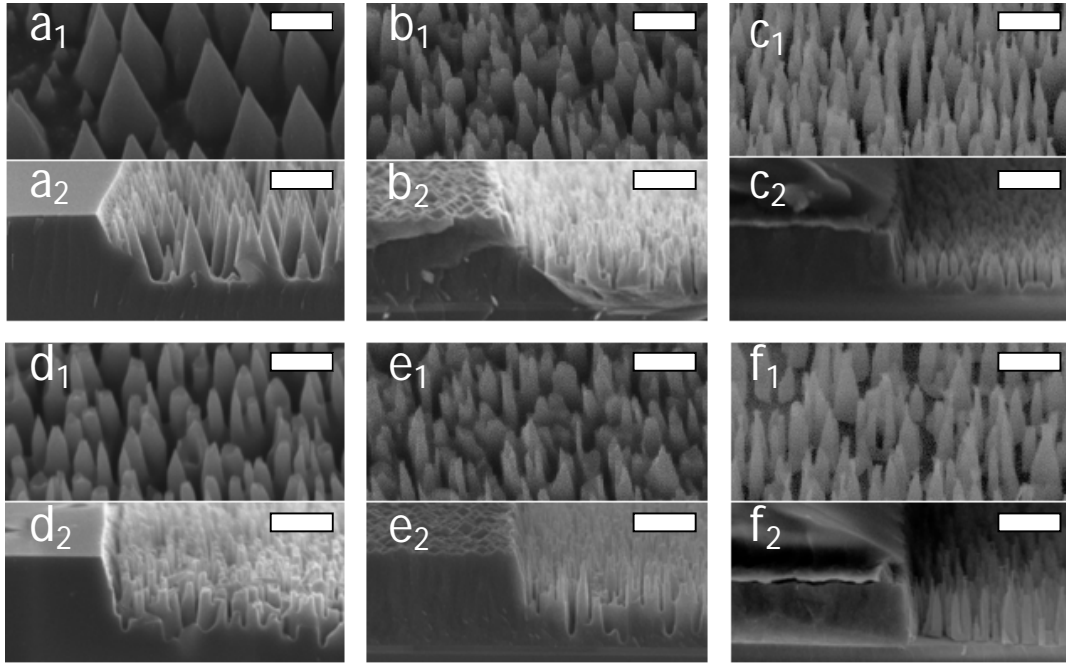


Figure 2: Representative SEM micrographs on the effect of wafer temperature on pillar morphology at various samples. The scale bar is 500 nm on each picture. Perspective views (index: 1) and cross-sectional views (index: 2) are recorded at tilt angles of 30° and 10° respectively. Samples in the first and second row were etched at -110°C and -100°C, respectively. c-Si samples: a) and d); poly-Si "A" samples: b) and e); poly-Si "B" samples: c) and f). Relevant common etching parameters are: $O_{2flow} = 15$ sccm, $P_{RF} = 3$ W, $P_{ICP} = 700$ W.

In the case of poly-crystalline samples there is a moderate decrease in pitch density, while pillar height apparently does not change. Meanwhile, c-Si samples are particularly sensitive to temperature, as pitch density and pillar height significantly change at -100°C.

Samples	Temperature (°C)	Pitch density (site/ μm^2)	Pillar height (nm)
Poly-Si "A"	-110	27.2±8.2	708±50
c-Si		7.6±2.5	1039±39
Poly-Si "A"	-100	26.1±6.2	752±97
c-Si		22.5±5.9	700±157
Poly-Si "A"	-90	18±3.7	770±102
c-Si		20.8±4.7	719±116

Table 2: Relationship between wafer temperature, pitch density and pillar height. Relevant common etching parameters are O_2 flow = 15 sccm, $P_{RF} = 3$ W, $P_{ICP} = 700$ W

3.1.2 Oxygen flow rate

O₂ flow rate is a dominant factor in the formation of passivation layers during cryogenic etching of Si in SF₆/O₂ plasma [Jansen, 2009]. Besides etch rate, anisotropy is also influenced by O₂ content due to the intensity of sidewall passivation mechanism. Effect of O₂ flow rate on morphology is illustrated by Fig. 3 and quantitative evaluation is summarized in Table 3. Increasing the SF₆/O₂ ratio causes smaller pitch density and larger etch rate in c-Si substrate compared to the case of poly-Si layers. In case of poly-Si "B" both pillar density and pillar height are less sensitive to O₂ flow, and pillar height is particularly more uniform than that of poly-Si "A" or c-Si samples.

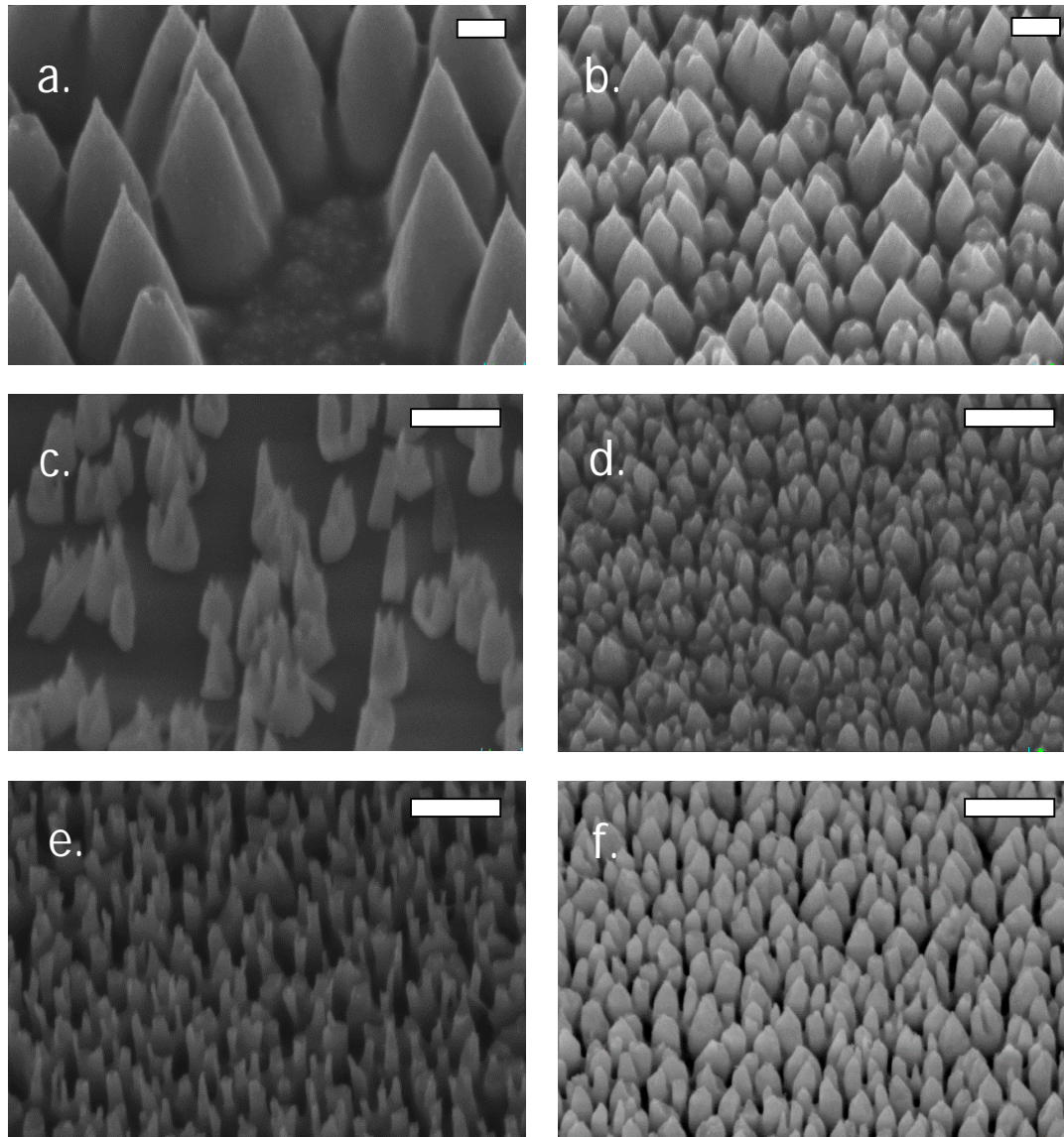


Figure 3: Representative SEM micrographs on the effect of O₂ flow on pillar morphology. Scale bar is 200 nm on each picture. Samples in the first and second column were etched at 10 sccm and 15 sccm of O₂ flow, respectively. c-Si samples: a) and b); poly-Si "A" samples: c) and d); poly-Si "B" samples: e) and f). Relevant common etching parameters are: $T = -110^{\circ}\text{C}$, $P_{\text{RF}} = 2 \text{ W}$, $P_{\text{ICP}} = 700 \text{ W}$

Samples	O ₂ flow (sccm)	Pitch density (site/μm ²)	Pillar height (nm)
<i>c-Si</i>	10	2.4±0.6	1973±131
	15	22.1±6.7	690±76
<i>Poly-Si "A"</i>	10	9.4±2.2	783±116
	15	39.3±13	422±130
<i>Poly-Si "B"</i>	10	47.3±5.3	482±13
	15	71.7±14	355±6

Table 3: Relationship between O₂ flow, pitch density and pillar height. Relevant common etching parameters are: $T = -110^{\circ}\text{C}$, $P_{RF} = 2\text{ W}$, $P_{ICP} = 700\text{ W}$

3.1.3 Radio frequency power

The radio frequency power corresponds to the plasma bias, which determines the physical component of dry etching through controlling ion energy. It seems obvious that increasing the ion energy is accompanied by increasing anisotropy, and eventually promoting the formation of sharp pillars with increased etch rate. In our experiments, we used RF power below 4 W, in order to decrease ion angular distribution and therefore minimizing the thickness of the dark sheath field, which corresponds to the formation of more vertical structures [Jiang, 2012]. Our findings on relationship between RF power and morphology are summarized in Fig 4. and Table 4.

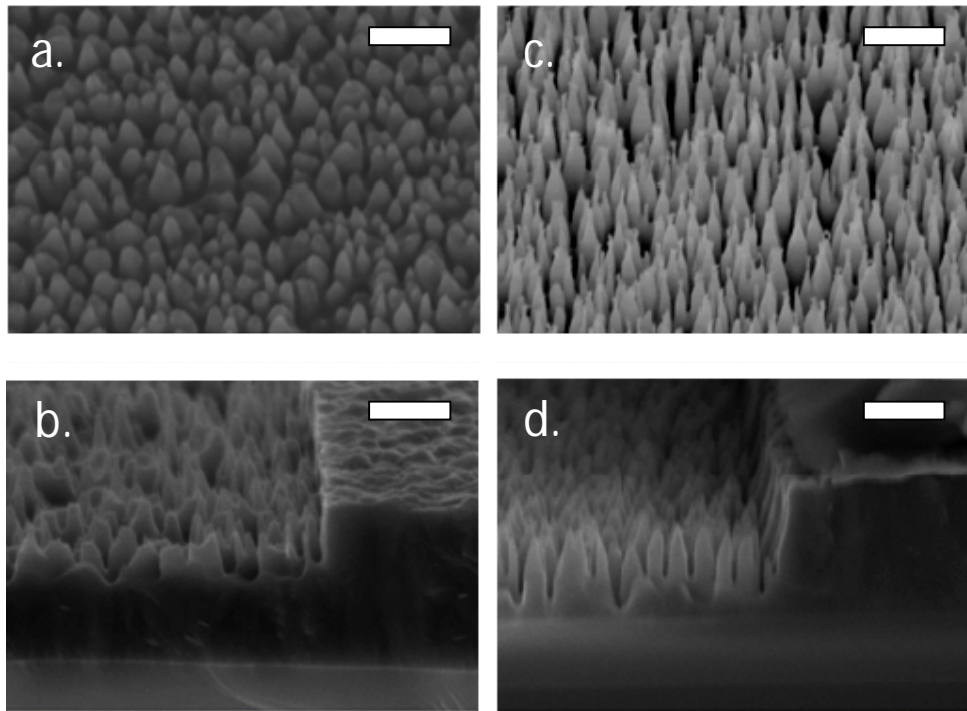


Figure 4: Representative SEM micrographs of poly-Si "B" samples formed at different RF power: a) and b) 2 W, c) and d) 3 W. Scale bar is 500 nm on each picture. Relevant etching parameters in both cases are: $SF_{6\text{ flow}}: 40$

$ccm, O_{2\ flow}: 15\ sccm, T = -110^{\circ}C, P_{ICP} = 700\ W$

RF power	Morphology parameters	Poly-Si "A"	Poly-Si "B"	c-Si
2 W	Pillar density (site/ μm^2)	39.3 \pm 13	71.7 \pm 14	22.1 \pm 6.7
	Pillar height (nm)	422 \pm 130	355 \pm 6	690 \pm 76
3 W	Pillar density (site/ μm^2)	27.2 \pm 8.2	39.4 \pm 9.1	7.6 \pm 2.5
	Pillar height (nm)	708 \pm 50	528 \pm 121	1039 \pm 39

Table 4: Comparison between the morphology of single crystalline and poly-crystalline Si samples as a function of RF power. Relevant etching parameters are: $SF_6\ flow: 40\ sccm, O_2\ flow: 15\ sccm, T = -110^{\circ}C, P_{ICP} 700\ W$

3.2 Effect of exposed area

3.2.1 Microloading

Proper knowledge on the effect of microloading is essential, since the presence of densely packed patterned arrays - unlike in the case of laser pulse method [Her, 1998; Vorobyev, 2011] - may deteriorate the BPS uniformity throughout the wafer due to etch rate difference caused by pattern density [Jansen, 1995]. This fact is particularly interesting for sensor design as the uniformity of a transducer area based on a possible BPS seed layer is crucial. Representative micrographs on BPS arrays of different pitch size and distances are illustrated in Fig. 5.

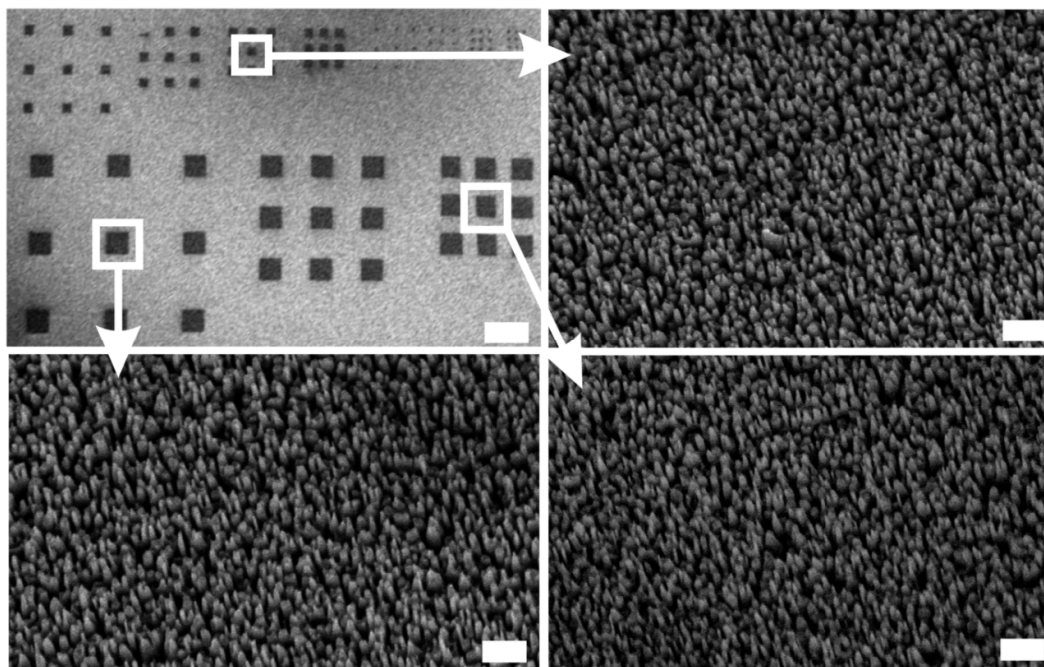


Figure 5: Morphology of BPS at several microloading situations. Scale bar represents 200 μm (overview SEM picture) and 200 nm (close SEM views).

3.2.2 Macroloading

Macroloading in reactive ion etching is a major concern regarding inhomogeneity in etch rate throughout the silicon wafer. In order to demonstrate the sensitivity of morphology to macroloading, wafers containing 10% and 90% of exposed poly-silicon surfaces were investigated. Our observations are summarized in Fig. 6. Our results suggest that dimensions of macroscale topology is quite limited since higher exposed area corresponds to higher etch rate, while a gradient in pillar density can be also noticed close to the edges of the micropatterns.

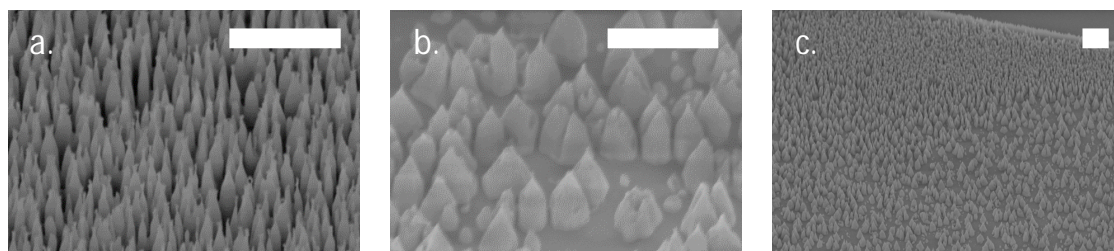


Figure 6: Effect of macroloading on BPS formation. a) and b) represents cases at a loading of 10% and 90% respectively, while c) shows a gradient in pillar density close to the edge of the patterned area. Scale bar represents 1 μm . Relevant etching parameters are: SF_6 flow = 40 sccm, O_2 flow = 15 sccm, $T = -110^\circ\text{C}$, $P_{\text{RF}} = 3 \text{ W}$, $P_{\text{ICP}} = 700 \text{ W}$.

3.3 Measurements on grain structure

Representative AFM images of both poly-crystalline thin film layers are illustrated in Fig. 7. Difference in grain size is apparent. The measured RMS roughness of sample poly-Si "A" and "B" are 34.8 nm (max. size: 256 nm) and 24.5 nm (max. size: 187 nm) respectively.

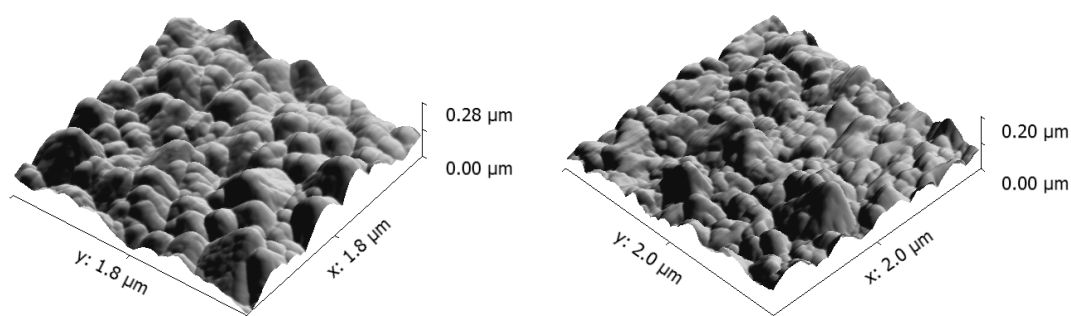


Figure 7: Representative AFM pictures on the surface roughness of poly-Si „A“ and poly-Si "B"

The X-ray diffraction images of both poly-silicon layers are demonstrated in Fig. 8. In the sample poly-Si "A", crystalline orientation of (110) is dominant, while poly-Si "B" is featured by a balanced (111) and (110) texture.

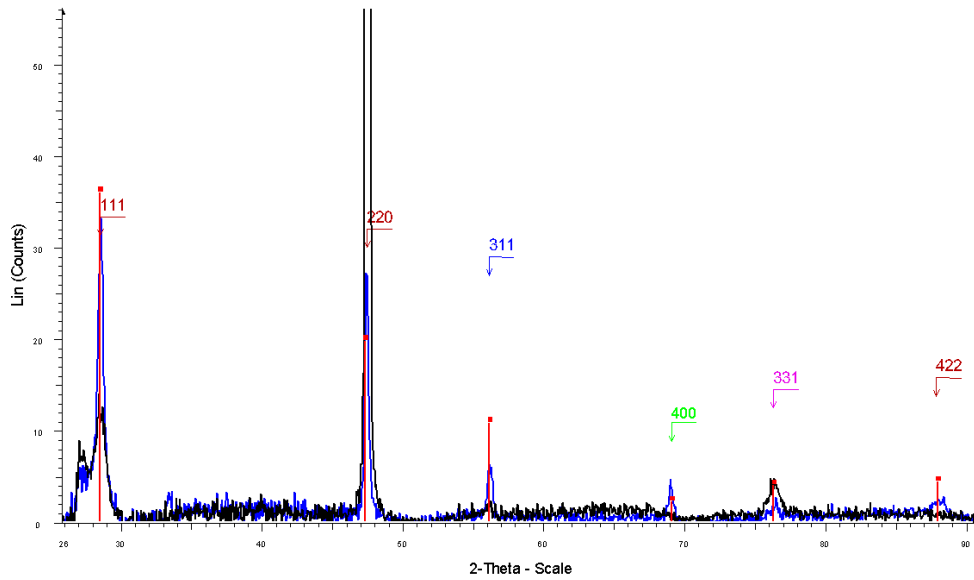


Figure 8: Evaluation of XRD image. Poly-Si „A” (black), poly-Si „B” (blue) and silicon powder as reference (red) are illustrated.

3.4 Surface enhancement by subsequent metallization

Impedance spectroscopy based devices, potential sensors or fuel cells need large specific surface area Pt sites. A basic application of the proposed BPS structures is the utilization of the enhanced specific surface area by subsequent metallization. The proposed fabrication technique integrated in the process flow of a microelectrode array and SEM images of a nanostructured, Pt covered microelectrode site is shown on Fig.9 a and b, respectively.

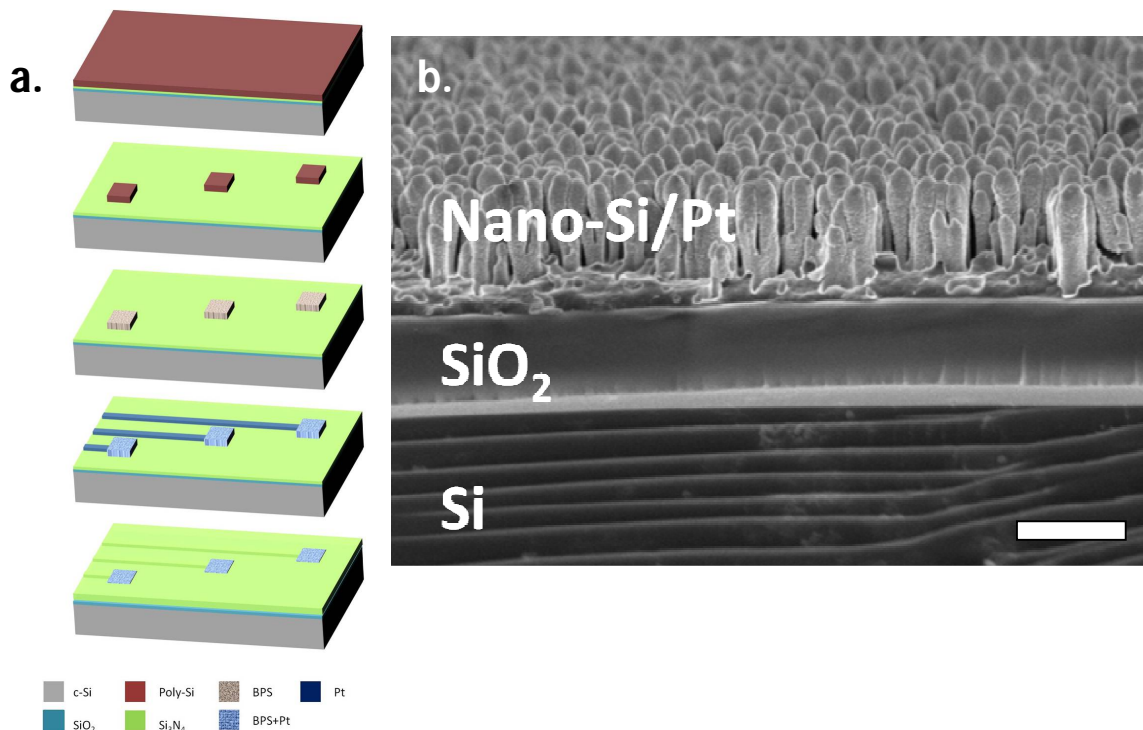


Figure 9: a) Schematic process flow of a microelectrode array with BPS steps (LPCVD deposited poly-Si on insulating $\text{SiO}_2/\text{Si}_3\text{N}_4$ stack, micropatterning of poly-Si via photolithography and subsequent wet etch, BPS formation on the microstructured area, metallization and subsequent patterning of metal lines and pads with lift-off, passivation by LPCVD deposited Si_3N_4 and contact opening); b) BPS layer covered with Ti/Pt. The micrograph of the uncovered sample is shown in Fig. 2.e Relevant etching parameters are: SF_6 flow = 40 sccm, O_2 flow = 15 sccm, $T = -100^\circ\text{C}$, $P_{\text{RF}} = 3 \text{ W}$, $P_{\text{ICP}} = 700 \text{ W}$.

BPS layers covered by 15 nm Ti and 100 nm platinum were investigated by electrochemical techniques like CV and EIS in order to reveal the increase in specific surface area (SSA) due to nanostructuring contact surfaces for application in potential sensors. Fig. 9 shows the cross-section of a sputtered sample.

Representative CV and EIS curves are shown in Fig. 10 and 11. Significant surface enhancement is observed in the case of samples fabricated by several recipes. The change in specific surface area (SSA) of metalized BPS compared to reference sputtered platinum thin film is summarized in Table 5. The highest increase in SSA achieved was 44 times that of the reference surface.

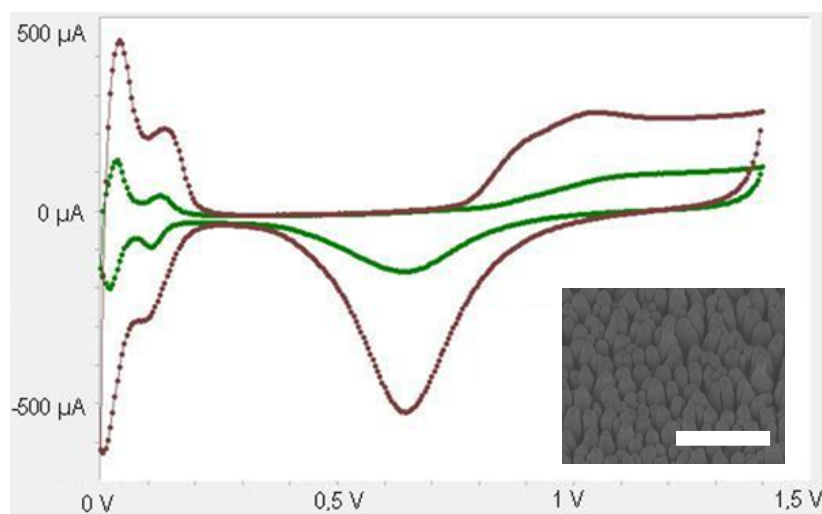


Figure 10: Representative CV curves for a reference SiO_2 (green) and BPS layer (red - see inset for SEM view) both covered with 15 nm / 100 nm thick Ti/Pt. Scale bar is $1 \mu\text{m}$. Relevant etching parameters of BPS seed layer are: SF_6 flow = 40 sccm, O_2 flow = 20 sccm, $T = -90^\circ\text{C}$, $P_{\text{RF}} = 2 \text{ W}$, $P_{\text{ICP}} = 700 \text{ W}$.

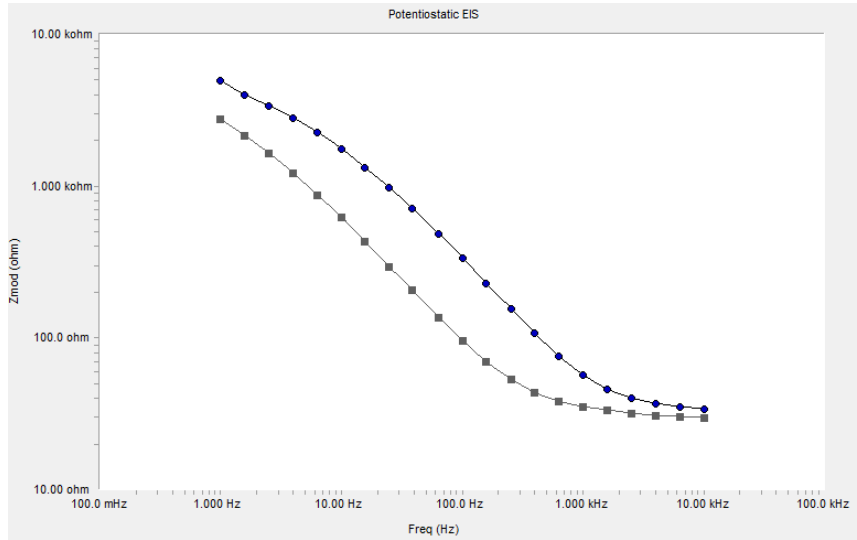


Figure 11: Representative EIS curves for a reference SiO₂ (circular dots) and BPS layer (rectangular dots) both covered with 15 nm / 100 nm thick Ti/Pt. Scale bar is 1 μm. Relevant etching parameters of BPS seed layer are: SF₆ flow = 40 sccm, O₂ flow = 15 sccm, T = -90°C, P_{RF} = 2 W, P_{ICP} = 700 W.

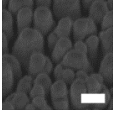
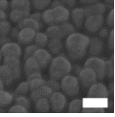
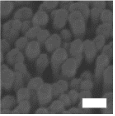
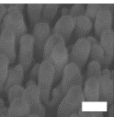
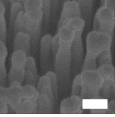
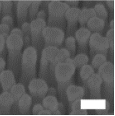
O ₂ flow rate (sccm)	Temperature (°C)	RF power (W)	SEM view	Relative change in SSA
10	-110	1		7.83
15	-110	2		12.13
15	-90	2		18.55
10	-110	2		26.17
15	-100	3		33.04
15	-110	3		44.2

Table 5: Relative change of specific surface area with respect to different fabrication parameters. Each metalized BPS surface is shown in SEM micrographs. Scale bar is 100 nm.

4 Discussion

4.1 Effect of etching parameters on BPS formation

4.1.1 Temperature

According to Fig. 2, a slight decrease in temperature causes a remarkable change in black c-Si morphology. Pillar density becomes almost three times higher at -100°C than at -110°C . This is probably caused by the lower rate of inhibitor formation. In the case of poly-Si samples it seems that a preferential etching takes place which is rather influenced by grain orientation than by temperature or initial surface roughness (see Fig. 2). In this case, the dominant content of (110) orientation crystals in poly-Si "A" corresponds to this preferential manner with no statistically significant change in either pillar density or pillar height. On the other hand, findings on poly-Si "B" shows that increasing the (111)/(100) ratio in grain orientation tends to decrease pillar density, while average pillar height is not changed significantly. This observation is generally opposite to the case of c-Si, where directionality apparently decreases with temperature [Jansen, 2010]. Since this is the first time, when plasma etching of poly-Si in SF_6 chemistry was investigated, the precise formation mechanism in the examined temperature range cannot be reliably predicted based on the available data set.

4.1.2 Oxygen flow

Si etch rate is generally decreasing as O_2 flow is increased at constant SF_6 flow [Yoo, 2009; Jiang, 2012]. This trend is noticed throughout the experiments, however, the ratio of crystal orientations present in PBS layers seems to have dominant effect on pillar formation. Considering the result of SEM and XRD analysis, it can be concluded that a balanced ratio of (110) and (100) orientation (poly-Si "B") results in significantly lower standard deviation in pillar height values, while the decrease in pillar density due to increased O_2 flow rate can be reduced from approximately 85% down to 35% compared to c-Si.

4.1.3 RF power

Directionality of etching in case of all our samples increased as RF power increased, which is in good agreement with previous findings on the effect of plasma bias on etching anisotropy in c-Si substrates [Moreno, 2010; Jansen, 2010]. On the other hand, it is obvious that poly-crystalline Si samples have an inherent influence on pitch density, which does not decrease as drastically as experienced in the case of c-Si samples. Smaller grain size (poly-Si "B") deteriorates this effect, which is possibly caused by the synergetic behavior of physical and chemical compounds of etching as the density of grain boundaries increases. Eventually, it should be noted that in our experiments there is an insulator thin film (SiO_2) below poly-Si, which is supposed to have a secondary charging effect due to ion bombardment as etching is gradually advancing to the interface of SiO_2 /poly-Si thin films.

4.1.4 Exposed area

According to the microanalysis, etch rate in our cryogenic process apparently does not depend on microloading in case of 1 μm poly-Si thickness. This means that microscale topology (e.g. density of biosensor arrays based on BPS seed layer) can be virtually arbitrary.

4.2 Poly-silicon grain structure - further opportunities for tuning morphology

Since the grain structure of poly-Si is inherently determines the morphology of BPS thin films, altering the process parameters of LPCVD deposition gives further opportunities to control crystalline properties of the base layer and characteristics of the nanostructure. Generally, the degree of crystallinity, the grain size and the ratio of grain orientations in the film are affected by temperature and chamber pressure [Kamins, 1998; Modreanu, 2004]. Moreover, subsequent annealing of the poly-Si thin films can also change the ratio of (111), (220) and (311) orientation crystals substantially [Lysacek, 2010], which might be also a powerful tool to control BPS morphology beneficially as our results in this section revealed.

4.3 Application in potential sensors

The demonstrated specific surface area improvement (7-44x) using platinized BPS is in the same range as the surface enhancement achieved by Pt grey formation [Zhao, 2005]. Microelectrode arrays covered by platinized BPS are suitable to act as a recording and even stimulating electrode in biological media. Pt has the preferred capacitive charge injection mechanism and using BPS as a nanostructured seed layer the charge injection factor can be enhanced to the similar level as fractal TiN, carbon nanotubes or IrOx sensing layers have [Cogan, 2008], moreover, the fabrication of metalized BPS sensing structure fits to the conventional MEMS process flow. Beside the impedance reduction and charge injection enhancement, BPS is a suitable candidate for controlled electrical interaction with single cells in impedance spectroscopy based lab-on-a-chip systems due to the strong electrical field emitting capability of the sharp tips which can locally depolarize cell membranes [Xie, 2012; Mohammad, 2014].

4.4 Further possible applications

Since our proposed microfabrication method of black poly-silicon seed layer offers high flexibility due to being micromachined on top of any dielectric or semiconductor thin film, we envision that the functionality of several MEMS sensor will benefit from its versatility in many fields. The increased specific surface area can be utilized in either chemical sensors to promote catalytic reactions [Jemenez-Cadena, 2007; Roumanie, 2008] or to increase signal-to-noise ratio in potential sensors [Joye, 2009]. Since the nanostructure and thickness of BPS can be tailored, the optical properties (reflectance, absorbance) can also be influenced, and e.g. radiation sensors can utilize it as absorbent film. Finally, progress in revealing biocompatibility in cell-microdevice interface suggests that silicon nanostructuring can beneficially influence cell adhesion [Turner, 1997; Moxon, 2004] and growth [Delivopoulos, 2009], which can be cell-specifically designed using BPS. In the above examples BPS can be applied both as seed layer, sacrificial layer or functional material.

5 Conclusion

In our work, BPS fabrication was demonstrated on the surface of thermally oxidized Si by reactive ion etching at cryogenic temperature. Etching parameters like temperature, O₂ flow and RF power were varied and morphology of the resultant thin film was evaluated by SEM.

Increasing the SF₆/O₂ ratio causes smaller pitch density and larger etch rate in c-Si substrate compared to that of poly-silicon layers. In case of poly-Si "B", both pillar density and pillar height are less sensitive to O₂ flow. Pillar height is particularly more uniform than that of poly-Si "A" or c-Si samples. Considering the results of SEM and XRD analysis, it can be concluded that a balanced ratio of (110) and (100) orientation (poly-Si "B") results in significantly lower standard deviation in pillar height values, while the decrease in pillar density due to increased O₂ flow rate can be reduced from approximately 85% down to 35% compared to c-Si.

As temperature goes up, there is a moderate decrease in pitch density, while pillar height practically does not change in the case of poly-Si samples. On the other hand, c-Si samples are particularly sensitive to temperature, as pitch density and pillar height significantly change at -100 °C. The dominant content of (110) orientation crystals in poly-Si "A" corresponds to this preferential manner with no statistically significant change in either pillar density or pillar height. Findings on poly-Si "B" shows that increasing the (111)/(100) ratio in crystallographic orientation results in decreasing pillar density, while average pillar height is not changed significantly.

According to our microanalysis, etch rate in our cryogenic process is not apparently dependent from microloading in case of 1 μm poly-Si thickness. This means that microscale topology (e.g. density of biosensor arrays based on BPS seed layer) can be virtually arbitrary. By controlling the crystalline properties (crystallinity, grain size, grain orientation) of poly-silicon layer during LPCVD deposition process, there is further room for tuning the final nanostructure of the BPS layer.

We proved how metalized BPS seed layer can be integrated in the process flow of a basic potential sensor and contribute to the increase in specific surface area in a controlled manner and therefore how can we reduce impedance of potential sensor surfaces.

BPS seed layer is envisioned to have a growing contribution to the field of biological and chemical sensors due to its highly tunable morphology and integrable fabrication technology.

6 Acknowledgement

The authors are grateful to the supportive staff of the MEMS Lab in RCNS, HAS. The assistance of Dr Zs Horvath in XRD measurements and Mr A Straszner in deep reactive ion etching is also acknowledged. A. Pongrácz and Z. Fekete are thankful for the Bolyai János Grant of the HAS and the Post-doctoral Research Grant of the HAS, respectively.

7 References

Abdolahad, M., Shashaani, H., Janmaleki, M., Mohajezadeh, S., Silicon nanograss based impedance biosensor for label free detection of rare metastatic cells among primary cancerous colon cells,

suitable for more accurate cancer staging, *Biosensors and Bioelectronics*, 2014, <http://dx.doi.org/10.1016/j.bios.2014.02.079>

Barberoglou, M., Zorba, V., Pagozidis, A., Fotakis, C., Stratakis, E., Electrowetting properties of micro/nanostructured black silicon, *Langmuir* 26 (2010), 13007-13014

Cogan S.F., Neural Stimulation and Recording Electrodes, *Annual Review of Biomedical Engineering*, 10 (2008) 275-309-

Delivopoulos, E., Murray, A.F., MacLeod, N.K., Curtis, J.C., Guided growth of neurons and glia using microfabricated patterns of parylene-C on a SiO₂ background, *Biomaterials* 30 (2009) 2048-58.

Dorrer, C., R uhe, J., Wetting of Silicon Nanograss: From Superhydrophilic to Superhydrophobic Surfaces, *Adv. Mater.* 20 (2008) 159–163.

Du, J., Blanche, T.J., Harrison, R.R., Lester, H.A., Masmanidis, S.C., Multiplexed, High Density electrophysiology with Nanofabricated Neural Probes, *PLOS ONE* 6 (2011) e26204

Gharghi, M., Sivoththaman, S., Formation of nanoscale columnar structures in silicon by a maskless reactive ion etching process, *J. Vac. Sci. Technol. A* 24 (2006) 723-727.

Her, T-H., Finlay, R. J., Wu, C. , Deliwala, S., Mazur, E., Microstructuring of silicon with femtosecond laser pulses, *Appl. Phys. Lett.* 73 (1998) 1673.

Hoyer, P., Theuer, M., Beigang, R., Kley, E-B., THz emission in b-Si: Terahertz emission from black silicon, *Appl. Phys. Lett.* 93 (2008) 091106

Jansen, H., de Boer, M., Legtenberg, R., Elwenspoek, M., The black silicon method: a universal method for determining the parameter setting of a fluorine-based reactive ion etcher in deep silicon trench etching with profile control, *J. Micromech. Microeng.* 5 (1995) 115-120.

Jansen, H.V., de Boer, M.J., Unnikrishnan, S., Louwense, M.C., Elwenspoek, M.C., Black silicon method X: a review on high speed and selective plasma etching of silicon with profile control: an in-depth comparison between Bosch and cryostat DRIE processes as a roadmap to next generation equipment, *J. Micromech. Microeng.* 19 (2009) 033001

Jansen, H.V., de Boer, M.J., Ma, K., Giron es, M., Unnikrishnan, S., Louwense, M.C., Elwenspoek, M. C., Black silicon method XI: oxygen pulses in SF₆ plasma, *J. Micromech. Microeng.* 20 (2010) 075027

Jimenez-Cadena, G., Riu, J., Rius, F. X., Gas sensors based on nanostructured materials, *Analyst* 132 (2007) 1083–1099.

Joye, N., Schmid, A., Leblebici, Y., A Cell-Electrode Interface Noise Model for High-density Microelectrode Arrays, 31st Annual International Conference of the IEEE EMBS, Minneapolis, Minnesota, USA, September 2-6, 2009, pp. 3247-3250.

Kalem, S., Werner, P., Arthursson, O., Talalaev, V., Nilsson, B., Hagberg, M., Frederiksen, H., Sodervall, U., Black silicon with high density and high aspect ratio nanowhiskers, *Nanotechnology* 22 (2011) 235307

Kamins, T., Polycrystalline Silicon for Integrated Circuits and Displays. 2nd Ed., Kluwer Academic Publishers, Massachusetts, 1998.

Koynov, S., Brandt, M.S., Stutzmann, M., Black nonreflecting silicon surfaces for solar cells, *Applied Physics Letters* 88 (2006) 203107

Legtenberg, R., Jansen, H.V., de Boer, M.J., Elwenspoek, M.C., Anisotropic reactive ion etching of silicon using SF₆/O₂/CHF₃ gas mixtures, *Journal of the Electrochemical Society*, 142 (1995) 2020-2028.

Lysáček, D., Válek, L., Spousta, J., Šíkola, T., Špetík, R., Thermal stability of undoped polycrystalline silicon layers on antimony and boron-doped substrates, *Thin Solid Films* 518 (2010) 4052–4057.

Mao, H., Wu, W., Qian, C., Xu, J., Zhang, H., Silicon Nanopillar-forest based microfluidic surface-enhanced Raman scattering devices, *IEEE 24th International Conference on Micro Electro Mechanical Systems (MEMS)* (2011) pp. 968-971

Modreanu, M., Gartner, M., Cobianu, C., O'Looney, B., Murphy, F., Optical properties of silicon thin films related to LPCVD growth condition, *Thin Solid Films* 450 (2004) 105-110.

Moreno, M., Daineka, D., Cabarrocas, P.R., Plasma texturing for silicon solar cells: From pyramids to inverted pyramids-like structures, *Solar Energy Materials & Solar Cells* 94 (2010) 733–737.

Moxon, K.A., Kalkhoran, N.M., Markert, M., Sambito, M.A., McKenzie, J.L., Webster, J.T., Nanostructured Surface Modification of Ceramic-Based Microelectrodes to Enhance Biocompatibility for a Direct Brain-Machine Interface, *IEEE Transactions on Biomedical Engineering* 51 (2004) 881-889.

Pereira, J., Pichon, L.E., Dussart, R., Cardinaud, C., Duluard, C.Y., Oubensaid, E.H., Lefauchaux, P., Boufnichel, M., Ranson, P., *Appl. Phys. Lett.* 94 (2009) 07101

Roumanie, M., Delattre, C., Mittler, F., Marchand, G., Meille, V., de Bellefon, C., Pijolat, C., Tournier, G., Pouteau, P., Enhancing surface activity in silicon microreactors: Use of black silicon and alumina as catalyst supports for chemical and biological applications, *Chemical Engineering Journal* 135S (2008) S317–S326.

Schmidt, M. S., Hübner, J., Boisen, A., Nanopillars: Large Area Fabrication of Leaning Silicon Nanopillars for Surface Enhanced Raman Spectroscopy, *Advanced Materials* 24 (2012) OP10

Serpenguzel, A., Kurt, A., Inanc, I., Cary, J.E., Mazur, E., Black Si can be formed by shining femtosecond laser pulses on Si followed by thermal annealing, *J. Nanophoton.* 2 (2008) 021770

Stubenrauch, M., Fischer, M., Kremin, C., Stoebenau, S., Albrecht, A., Nagel, O., *J. Micromech. Microeng.* 16 (2006) 82-87.

Su, Y., Li S., Zhao G., Wu Zh., Yang Y., Li W., Jiang Y., Optical properties of black silicon prepared by wet etching, *J Mater Sci: Mater Electron* 23 (2012) 1558–1561

Turner, S., Kam, L., Isaacson, M., Craighead, H. G., Shain, W., Turner, J., Cell attachment on silicon nanostructures, *J. Vac. Sci. Technol. B* (1997) 2848-2854.

Vorobyev, A.Y., Guo. C., Direct creation of black silicon using femtosecond laser pulses, *Applied Surface Science* 257 (2011) 7291–7294.

Walker, M.J., Comparison of Bosch and cryogenic processes for patterning high aspect ratio features in silicon, *Proceedings of SPIE* 4407 (2001) 89-99.

Xie, Ch., Lin Z, Hanson L., Cui Y., Cui B. Intracellular recording of action potentials by nanopillar electroporation, *Nature Nanotechnology* 7 (2012) 185-190.

Yoo, J.S., Parm, I.O., Gangopadhyay, U., Kim, K., Dhungel, S. K., Mangalaraj, D., Yi, J., Black silicon layer formation for application in solar cells, *Solar Energy Materials and Solar Cells* 90 (2006) 3085-3093.

Zhang, T, Zhang, P., Li, S., Li, W., Wu, Z., Jiang, Y., Black silicon with self-cleaning surface prepared by wetting processes, *Nanoscale Res Lett.* 8 (2012) 351

Zhou D.M., Platinum electrode and method for manufacturing the same, (2005), US 6974533 B2